Surfactant-templating strategy for ultrathin mesoporous TiO₂ coating on flexible graphitized carbon supports for high-performance lithium-ion battery

Yong Liu [a,1], Ahmed A. Elzatahry [b,1], Wei Luo [a,c,1], Kun Lan [a,1], Pengfei Zhang [a,d,1], Jianwei Fan [a,e], Yong Wei [a], Chun Wang [a], Yonghui Deng [a], Gengfeng Zheng [a], Fan Zhang [a], Yun Tang [a], Liqiang Mai [d], Dongyuan Zhao [a,*]

[a] Department of Chemistry, Shanghai Key Laboratory of Molecular Catalysis and Innovative Materials, State Key Laboratory of Molecular Engineering of Polymers, Laboratory of Advanced Materials, iChEM (Collaborative Innovation Center of Chemistry for Energy Materials), Fudan University, Shanghai 200433, PR China
[b] Materials Science and Technology Program, College of Arts and Sciences, Qatar University, P.O. Box 2713, Doha, Qatar
[c] State Key Laboratory for Modification of Chemical Fibers and Polymer Materials, College of Materials Science and Engineering, Donghua University, Shanghai 201620, PR China
[d] State Key Laboratory of Advanced Technology for Materials Synthesis and Processing, Wuhan University of Technology, Wuhan 430070, Hubei, PR China
[e] College of Environmental Science and Engineering, State Key Laboratory of Pollution Control and Resource Reuse, Tongji University, Shanghai 200092, PR China

ARTICLE INFO

ABSTRACT

The electrochemical performance of nanocomposites could greatly be improved by rationally designing flexible core-shell heterostructures. Typically, the uniform coating of a thin mesoporous crystalline transition metal oxide shell on flexible graphitized carbon supports can provide both fast ion and electron transport pathways, which is an ideal material for high-performance lithium-ion batteries. Herein, we report a surfactant-templating assembly coating method to deposit an ultrathin mesoporous crystalline TiO₂ shell on flexible graphitized carbon supports by using amphiphilic triblock copolymer Pluronic F127 as a template. Taking multi-wall carbon nanotubes (CNTs) as an example support, the obtained flexible CNTs@mTiO₂ hybrid mesoporous nanocables exhibit an ultra-high surface area (~137 m²/g), large internal pore volume (~0.26 cm³/g), uniform accessible mesopores (~6.2 nm) and ultrathin highly-crystalline mesoporous anatase shells (~20 nm in thickness). As an anode material for lithium battery, the flexible CNTs@mTiO₂ hybrid mesoporous nanocables show high-rate capacity (~210 mA h g⁻¹ at 20 C, 1 C = 170 mA g⁻¹), high Coulombic efficiency (nearly 100% during 1000 cycles at 20 C) and ultralong-cycling life (keeping ~210 mAh g⁻¹ after 1000 cycles at 20 C). The strong synergistic coupling effect between CNT cores and thin mesoporous TiO₂ shells, high surface area, accessible large pores and highly crystalline thin mesoporous shells result in excellent performance in lithium batteries. This versatile surfactant-templating assembly coating method can be easily extended to deposit an ultrathin mesoporous TiO₂ layer on flat graphene (GR) to form a uniform sandwich-like flexible GR@mTiO₂ nanoflakes, which opens up a new opportunity for depositing thin mesoporous transition-metal oxides on graphitized carbon supports for advanced applications in energy conversion and storage, photocatalysis, sensors and drug delivery, etc.

1. Introduction

Development of high-performance lithium-ion batteries (LIBs) with a capacitor-like high rate and battery-like high capacity is highly demanded for the next generation electronic devices [1–16]. In this regard, improvement of both ion and electron transport kinetics in batteries is greatly needed [17–21]. From the materials perspective, a flexible coaxial core-shell heterostructures formed by coating an ultrathin mesoporous crystalline TiO₂ shell on flexible graphitized carbon supports can meet both criteria [22,23]. In this unique flexible coaxial core-shell hybrid architecture, each component synergistically serves a specific purpose. The graphitized carbon core can provide superior electronic conductivity and excellent mechanical flexibility

[10,24–27]. Meanwhile, the ultrathin mesoporous crystalline TiO_2 shells can in turn shorten Li^+ ions diffusion length and facilitate fast penetration of the electrolyte [28–30], which guarantee sufficient transport of both ions and electrons in high rate and capacity performance in lithium-ion batteries. Previously, many efforts have been directed toward synthesis of various CNT/TiO_2 hybrid materials. Typically, Wan et al. have reported a wet-chemical synthetic route to deposit disordered nanoporous TiO_2 shells onto CNT surface for efficient lithium storage [31]. Wang and co-workers have developed a PEO-aided self-assembly method to grow TiO_2 nanoparticles onto CNT surface as a high-rate anode [32]. In addition, Lou and co-workers have developed a new hydrothermal method to direct grow TiO_2 nanosheets@CNTs coaxial nanocables with excellent lithium-storage performance [33]. We have also confirmed a sol-gel design strategy for ultra-dispersed TiO_2 nanoparticles on graphene for high-performance lithium ion batteries [34,35]. Though there are many papers concerning CNT/TiO_2 composites, very few work has succeeded in coating well ordered mesoporous TiO_2 shells on the surface of CNTs, yet. It is highly desirable for achieving fast rate and high capacity performance in lithium ion batteries.

Typically, direct coating of ultrathin mesoporous anatase TiO_2 shells with a highly crystalline framework and large-pore size on the entire surface of graphitized carbon supports is difficult to achieve, which attributes to two reasons primarily: (i) The large lattice mismatch and high interfacial energy on the curved interfaces between graphitized carbon supports and titanium crystals often allow the depositing of island-like TiO_2 domains on the surface of graphitized carbon, rather than a continuous and conformable mesoporous TiO_2 shell [36–39]. (ii) The high coordination number of titanium endows its precursor high reactivity, which makes it difficult to control the hydrolysis rate for heterogeneous nucleation and corresponding cooperative assembly with surfactants to grow a thin mesoporous shell with a highly-crystalline framework [40–42]. Therefore, it is of great importance and interest to develop a new method to controllably grow an ultrathin mesoporous anatase TiO_2 shell with large and accessible mesopores on the graphitized carbon supports by a surfactant-based coating process, so as to achieve the double goal of capacitor-like high rate and battery-like high capacity performance in lithium-ion batteries.

Taking CNTs as an example support, here we demonstrate a novel surfactant-templating assembly coating method to synthesize uniform CNTs@mTiO_2 core-shell hybrid mesoporous nanocables with flexible multi-wall CNT cores and ultrathin crystalline mesoporous anatase TiO_2 shells. To the best of our knowledge, it is the first time to synthesize uniform flexible CNTs@mTiO_2 hybrid mesoporous nanocables through a layer-by-layer spherical micelles depositing process within surfactant-templating assembly coating process. This method is also very simple and reproducible, yet important, which allows direct coating a uniform ordered mesoporous TiO_2 shell with spherical mesopores on various flexible graphitized carbon supports, highly desirable for achieving fast rate and high capacity performance in lithium ion batteries. Triblock copolymer Pluronic F127 ($PEO_{106}PPO_{70}PEO_{106}$) here is used as a template, tetrabutyl titanate (TBOT) as a titania precursor, ammonia as hydrolysis catalyst and ethanol/dimethyl formamide (DMF) as mixed solvent. The obtained flexible CNTs@mTiO_2 coaxial nanocables possess a high surface area (~137 m^2/g), large internal pore volume (~0.26 cm^3/g), highly-open large ordered mesopore (~6.2 nm) and thin crystalline anatase TiO_2 mesoporous shell (~20 nm in thickness). Lithium battery measurements show that the flexible CNTs@mTiO_2 hybrid mesoporous nanocable anodes can synergistically enhance Li^+ ion and electron transport kinetics, resulting in unusual superior electrochemical performance with high-rate capacity (213 mA h g^{-1} at 20 C), high Coulombic efficiency (nearly 100% during 1000 cycles at 20 C) and superior cycling stability (keeping reversible capacity about 210 mAh g^{-1} after 1000 cycles at 20 C).

2. Experimental section

2.1. Chemicals

The oxidized CNTs were purchased from Chengdu Organic Chemicals Co., LTD. Triblock copolymer Pluronic F127 ($M_w = 12600$, $PEO_{106}PPO_{70}PEO_{106}$) were purchased from Aldrich Corp. Concentrated HNO_3, KNO_3, $KMnO_4$, H_2O_2 (30 wt%), tetrabutyl titanate (TBOT), concentrated HCl, anhydrous ethanol and N, N-dimethyl formamide(DMF) were purchased from Sinopharm Chemical Reagent Co., Ltd. (Shanghai, China). Concentrated ammonia solution (28–30 wt%) and graphite were purchased from Sigma-Aldrich. All chemicals were used as received without further purification. Deionized water was used for all experiments.

### 2.2. Preparation of the oxidized CNT supports

The oxidized CNTs were prepared as follows: 0.1 g of raw multi-wall CNTs were suspended in 50 ml of concentrated nitric acid (68 wt%) and refluxed at 120 °C in an oil bath for 5 h. (*Caution:* Concentrated nitric acid is a corrosive solution, and appropriate safety precautions should be utilized including the use of acid resistant gloves and adequate shielding). After the mixture was cooled down to room temperature, it was filtered through a filter membrane with a pore diameter of 0.2 μm and washed with deionized water until the pH value of the filtrate was around 7.0. Then the product was dried at 60 °C for 12 h. This acid-pre-treatment could remove the caps of the carbon nanotubes as well as amorphous carbon. At the same time, surface oxygen groups such as carbonyl, carboxylic and ether could be produced onto the surfaces of the CNTs.

2.3. Synthesis of graphene oxide (GO)

The GO was synthesized from graphite *via* a modified Hummers method. Briefly, the commercial graphite (5.0 g) was added into a solution of concentrated H_2SO_4 (115 ml) cooled in an ice-water bath. KNO_3 (2.5 g) and $KMnO_4$ (15 g) were added very slowly (with a period more than 15 min) into the mixture. All the operations were carried out very slowly in a fume hood. The solution was allowed to stir in an ice-water bath for 2 h, then at 35 °C for 1 h. Then, 115 ml of water was added to the flask. After 1 h, 700 ml of water was added. After 15 min, the solution was removed from the oil bath and 50 ml of 30% H_2O_2 were added to end the reaction. This suspension was stirred at room temperature for 5 min. The suspension was then repeatedly centrifuged and washed twice with 5% HCl solution and then dialyzed for a week.

2.4. Synthesis of the mesoporous CNTs@mTiO_2 hybrid core-shell nanocables

The flexible mesoporous CNTs@mTiO_2 hybrid core-shell nanocables were prepared *via* surfactant-templating assembly coating method. Briefly, 20 mg of the oxidized CNTs obtained above was dispersed in a mixed solution containing 0.18 g of Pluronic F127, 30 ml of ethanol/DMF mixed solvent (20 ml of ethanol and 10 ml of DMF) and 0.07 ml of concentrated ammonia aqueous solution (28 wt%) to form a uniform dispersion. After stirring at room temperature for 3 h, 0.1 g of TBOT was added dropwise to the dispersion with continuous stirring. After the reaction for 6 h, the product was collected by centrifugation (8500 rpm for 15 min), leaving a colourless supernatant. The collected product was then washed with ethanol and water for three times, respectively. Finally, the dried mesostructured CNTs@ F127 micelles/TiO_2 hybrid nanocables were calcined under Ar at 400 °C for 2 h to remove the Pluronic F127 template, and the mesoporous CNTs@mTiO_2 hybrid nanocables were obtained. The sandwich-like flexible GR@mTiO_2 hybrid nanoflakes were prepared *via* the same
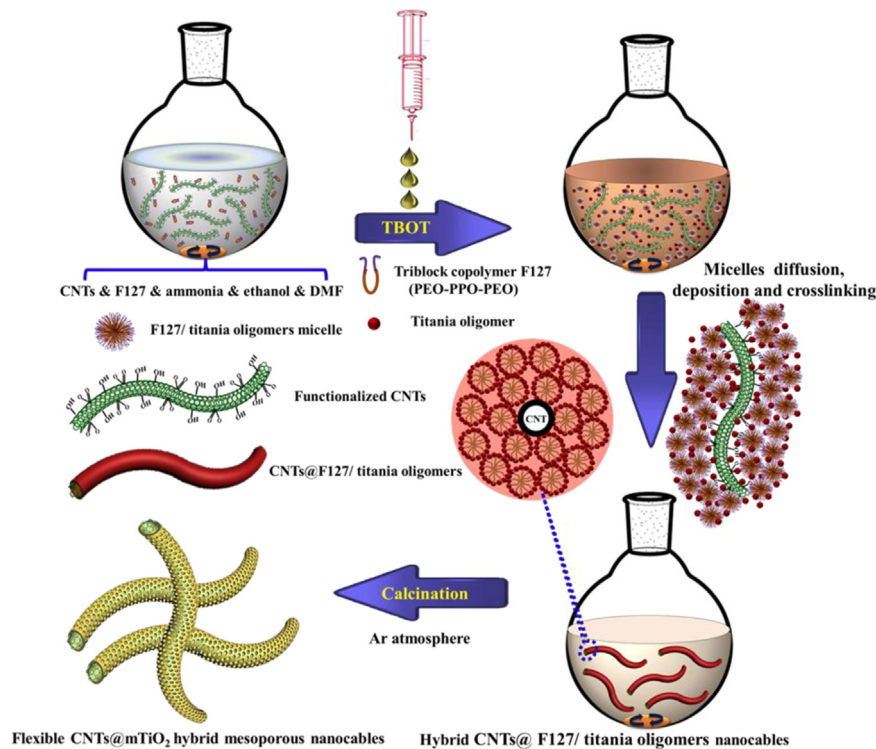
Fig. 1. Schematic representation of the surfactant-templating assembly coating approach for the preparation of the flexible CNTs@mTiO₂ hybrid mesoporous nanocables with a thin mesoporous anatase shell.

surfactant-templating assembly coating method strategy described above.

2.5. Materials characterization

Transmission electron microscopy (TEM) experiments were conducted on a JEOL JEM-2100F (UHR) microscope (Japan) operated at 200 kV. Energy-dispersive X-ray (EDX) and high-angle annular dark-field scanning TEM (HAADF-STEM) analyses were performed with a FEI Talos F200X electron microscope at 200 kV with an EDX detector system. The samples for TEM and EDX measurements were suspended ultrasonically in ethanol and supported onto a carbon-coated copper grid. X-ray diffraction (XRD) patterns were recorded with a Bruker D8 powder X-ray diffractometer (Germany) using Cu Kα radiation (40 kV, 40 mA). Small angle X-ray scattering (SAXS) measurements were taken on a Nanostar U small angle X-ray scattering system (Bruker, Germany) using Cu Kα radiation (40 kV, 35 mA). The d-spacing values were calculated by the formula $d=2\pi/q$. Nitrogen sorption isotherms were measured at 77 K with a Micromeritcs Tristar 3020 analyzer. All of the samples were degassed under vacuum at 180 °C for at least 8 h prior to the measurement. The Brunauer-Emmett-Teller (BET) method was utilized to calculate the specific surface areas using adsorption data in a relative pressure range from 0.05 to 0.25. The pore size distributions (PSD) were derived from the adsorption branch of the isotherms using the Barrett-Joyner-Halenda (BJH) model. The total pore volume (V_t) was estimated from the adsorbed amount at a relative pressure P/P_0 of 0.995. X-ray photoelectron spectroscopy (XPS) was recorded on an AXIS ULTRA DLD XPS System with MONO Al source (Shimadzu Corp.). Photoelectron spectrometer was recorded by using monochromatic Al K_R radiation under vacuum at 5×10^{-9} Pa. All of the binding energies were referenced to the C_{1s} peak at 284.6 eV of the surface adventitious carbon. Atomic force microscopy (AFM) measurements were taken using a Multimode in the tapping mode. The samples were deposited on a freshly cleaved mica surface. Raman spectra were collected by using Raman microscopes (Renishaw, UK) under 632.8 nm excitation.

2.6. Electrochemical tests

The electrochemical properties were evaluated by assembly of 2025 coin cells in an argon-filled glove box ($O_2 \leq 1$ ppm and $H_2O \leq 1$ ppm). Lithium pellets (China Energy Lithium Co., Ltd.) were used as the anode. The solution of $LiPF_6$ (1 M) in ethylene carbon (EC)/dimethyl carbonate (DMC) was used as electrolyte. The cathodes were obtained with 70% active material, 20% acetylene black and 10% poly (tetrafl uoroethylene) (PTFE). Then the mixed clay was rolled using a roller mill to form the freestanding film. And the film was cut into disk with a diameter of 8 mm. The loading of the active materials was 2–3 mg cm^{-2}. The specific capacity of the CNT@mTiO₂ hybrid mesoporous nanocables is calculated based on the total electrode mass. Galvanostatic charge/discharge cycling was studied with a multichannel battery testing system (LAND CT2001A). Cyclic voltammetric (CV) tests were conducted from 3.00 to 1.00 V using an electrochemical analyzer (Germany Instruments. Inc). The electrochemical impedance spectroscopy (EIS) was conducted using an electrochemical station (CHI 660).

3. Results and discussion

The procedure for the preparation of the flexible CNTs@mTiO₂ hybrid mesoporous nanocables is shown in Fig. 1. First, the multi-wall CNTs were functionalized with abundant carboxyl and hydroxyl groups by boiling in nitric acid, making them dispersible well in ethanol/DMF mixed solvent. Then, the spherical PEO-PPO-PEO/titania-oligomer composite micelles are formed *via* the hydrolysis and condensation of TBOT in a low content of concentrated ammonia (0.2 vol%), which are further deposited on the surface of the oxidized multi-wall CNTs through a layer-by-layer micelles depositing process. Transmission electron microscopy (TEM) images taken from the preparation solution show that these spherical composite micelles have a diameter of 8–10 nm, which is a typical core-shell structure with

PEO-PPO-PEO as the core and titania oligomers as the shell (Fig. S1). Finally, F127 templates were removed by calcination at 400 °C for 2 h in Ar atmosphere to form a mesoporous thin TiO$_2$ shell with a large pore size and highly crystalline anatase framework, resulting in well-defined flexible CNTs@mTiO$_2$ hybrid mesoporous nanocables.

The CNTs support after being functionalized by boiling in nitric acid have a diameter of ~20 nm and length of dozens of micrometres (Fig. S2), indicating that the nitric acid-pre-treatment does not change their morphology and flexibility. Then, a thin mesoporous TiO$_2$ shell with a thickness of about 20 nm are uniformly coated on entire functionalized CNTs *via* the surfactant-templating assembly coating process, resulting in uniform mesoporous core-shell CNTs@mTiO$_2$ hybrid nanocables (Fig. 2a). The feature of the ultrathin mesoporous TiO$_2$ shells is clearly revealed in the broken tips of nanocables in the SEM image (Fig. 2a, indicated by arrows). A high-resolution SEM (HRSEM) image of a single CNTs@mTiO$_2$ hybrid nanocable shows rough and porous surface with a diameter of approximately 80 nm (Fig. 2b). The ordered spherical mesopores are uniformly distributed on the entire rough surface of hybrid nanocables, and the average pore size is estimated to be ~5.8 nm. TEM images of the CNTs@mTiO$_2$ hybrid mesoporous nanocables (Fig. 2c) exhibit distinct core-shell hybrid structure with outer shell comprising numerous close-packed spherical mesopores. Such a pore arrangement model is further visually described in upper-left inset of Fig. 2c.

The high-resolution TEM image (HRTEM) recorded on the cross section of a single core-shell CNTs@mTiO$_2$ naocable shows that the highly crystallized mesoporous TiO$_2$ shells are closely integrated with CNTs (Fig. 2d and e). The cross-section TEM image also clearly reveals that the thickness of the mesoporous TiO$_2$ shells is as thin as~20 nm. The spacing of 0.338 nm estimated in the core area of the coaxial nanocables corresponds to the (002) crystalline plane of the multi-wall CNTs (Fig. 2e) [31]. Meanwhile, another spacing of 0.352 nm estimated in the mesoporous TiO$_2$ shells corresponds to the (101) planes of anatase (Fig. 2e) [43,44]. The HRTEM image taken along the CNTs@mTiO$_2$ mesoporous nanocables (Figs. 2f and S3) also clearly show the (101) and (002) anatase planes with an interfacial angle of 68.3° [45,46]. The selected-area electron diffraction (SAED) pattern recorded on a single core-shell CNTs@mTiO$_2$ nanocable (Fig. 2g) shows a series of clear spotty diffraction rings, which corresponds to the highly crystalline anatase phase [47]. The above SAED and HRTEM results well confirm that the mesoporous TiO$_2$ shells are highly crystalline anatase phase after calcination at 400 °C in Ar atmosphere.

The small-angle X-ray scattering (SAXS) pattern of the as-made CNTs@amorphous F127/TiO$_2$ hybrid nanocables (Fig. 2h) clearly shows three well-resolved diffraction peaks at q values of 0.070, 0.099 and 0.123 nm^{-1}, which can be indexed to the 110, 200 and 211 reflections of a body-centred cubic *Im3m* mesostructure, indicating that the spherical composite micelles are successfully coated on the surface of the oxidized CNTs *via* the surfactant-templating assembly coating method. After the removal of Pluronic F127 templates by calcination at 400 °C for 2 h in Ar, the CNTs@mTiO$_2$ hybrid mesoporous nanocables still shows three weak and broad scattering peaks at higher q values of 0.075, 0.106 and 0.130 nm^{-1}, obviously indicating that the cubic mesostructure is still retained. Nitrogen adsorption-desorption isotherms of the CNTs@mTiO$_2$ hybrid nanocables show characteristic type IV curves with distinguishable capillary condensation step (Fig. 2i). A distinct capillary condensation step at P/P$_0$=0.4–0.7 reflects characteristic mesopores. The pore size distribution calculated using the Barrett-Joyner-Halenda (BJH) model (inset of Fig. 2i) show two sets of pores. The primary pore size distribution centred at 6.2 nm is ascribed to the mesoporous TiO$_2$ shells, and the secondary pore size at 2.3 nm is probably attributed to CNTs (Inset of Fig. 2g). The Brunner-Emmet-Teller (BET) surface area and pore volume of the flexible CNTs@mTiO$_2$ hybrid mesoporous naocables are calculated to be as high as ~ 137 m^2/g and 0.26 cm^3/g, respectively.

Wide-angle X-ray diffraction (WXRD) of the pure CNTs shows four broad peaks of the 002, 101, 004 and 110 reflections, typical for crystalline graphite (Fig. 3(a)). After coating with the mesostructured F127/TiO$_2$ hybrid shells, the diffraction peaks corresponded to CNTs are seriously weakened, which is possibly attributed to the lower atomic number (Z) of carbon as well as the uniform amorphous F127/TiO$_2$ shell coating. After calcination at 400 °C for 2 h in Ar, the WXRD pattern of the CNTs@mTiO$_2$ hybrid mesoporous naocables exhibits the characteristic broad diffraction peaks at 2θ=25.4, 37.8, 48.0, 53.9, and 62.8°, which are indexed to the 101, 004, 101, 200, 105, and 204 diffractions of anatase (space group *I4$_1$/amd*) [40,41,44], respectively. The average crystal size is calculated to be~6.5 nm, in agreement with the domain size of the nanocrystals estimated from the HRTEM images. The high resolution X-ray photoelectron spectra (XPS) spectrum of C element (Fig. 3b) shows two sets of peaks. The main peak at the binding energy of 284.6 eV is assigned to adventitious carbon (C–C) [48,49]. The sharp peak located at 285.6 eV is assigned to be defect-containing sp^2-hybridized carbon (C=C) from CNTs [49,50], which is possibly attributed to the functionalization of the CNTs by boiling in nitric acid before the mesoporous TiO$_2$ shells are coated. The O1s XPS spectra (Fig. 3c) show three chemical states of oxygen. The sharp peak at 530.6 eV is assigned to the O–Ti bonds of mesoporous TiO$_2$ shells, indicating that the chemical state of oxygen in the mesoporous TiO$_2$ shells is mainly lattice oxygen. The other two peaks at 531.4 and 532.3 eV are assigned to O–H and O–C absorbed on the mesoporous TiO$_2$ shell surface [47]. The Ti2p XPS spectrum (Fig. 3d) reveals two sets of peaks at 465.2 eV (Ti2p$_{1/2}$) and 459.4 eV (Ti2p$_{3/2}$), which are slightly shifted to higher binding energy compared to those of bulk anatase. This shift implies a strong electron interaction between the mesoporous TiO$_2$ shells and CNT cores, and even partial formation of Ti-O-C bonds [51]. High-angle annular dark-field scanning TEM (HAADF-STEM) image of a single CNTs@mTiO$_2$ hybrid mesoporous nanocable clearly reveals the core-shell mesostructure with a CNT core and mesoporous TiO$_2$ shell (Fig. 3e). The elemental mapping from the HAADF-STEM image shows that only Ti, O and C elements are uniformly distributed on the whole hybrid nanocable (Figs. 3f–h and S4), further confirming that a pure mesoporous anatase TiO$_2$ shell is coated on the curved surface of CNTs.

In this surfactant-templating coating strategy, it is found that the amphiphilic Pluronic F127 and ammonia content here play significant roles in uniform mesoporous TiO$_2$ shell coating. Without amphiphic triblock copolymer F127 template, only a layer of the anatase TiO$_2$ nanoparticle (NPs) are deposited on the surface of the multi-wall CNTs (designated as CNTs@TiO$_2$ NPs) (Fig. S5). The TEM and HRTEM images reveal that each shell of the CNTs@TiO$_2$ NPs is composed of numerous close-packed anatase TiO$_2$ NPs with a size of~20 nm (Fig. S5b and S5c), no apparent mesopores can be observed between the compact anatase TiO$_2$ NPs. For the ammonia parameter, when the concentration of ammonia below 0.2 vol%, no obvious mesoporous TiO$_2$ shell are formed on the surface of CNTs (Fig. S6). Once the content of 0.2 vol% ammonia is reached, uniform thin mesoporous TiO$_2$ shells are coated on the surface of CNTs (Fig. 1). As the ammonia concentration increases to 0.3 vol%, the thickness of mesoporous TiO$_2$ shell increases to be about 60 nm (Fig. S7). This reveals that the higher ammonia concentration can increase the hydrolysis and condensation rate of TBOT, thus resulting in an increase of spherical PEO-PPO-PEO/titania oligomer micelles for TiO$_2$ shell coating [52,53]. However, when ammonia concentration is further increased to 0.4 vol%, some irregular mesoporous TiO$_2$ nanospheres organized from TiO$_2$ nanoparticles are formed in the reaction system (Fig. S8).

Based on the above observations, we propose a surfactant-templating assembly coating process for the uniformly coating of the ultrathin mesoporous anatase TiO$_2$ shells on the functionalized surface of multi-wall CNTs (Fig. 1). At a low concentration of weak base (0.2 vol% ammonia), TBOT molecules can slowly be hydrolysed and cross-linked to form titania oligomers. The oligomers can
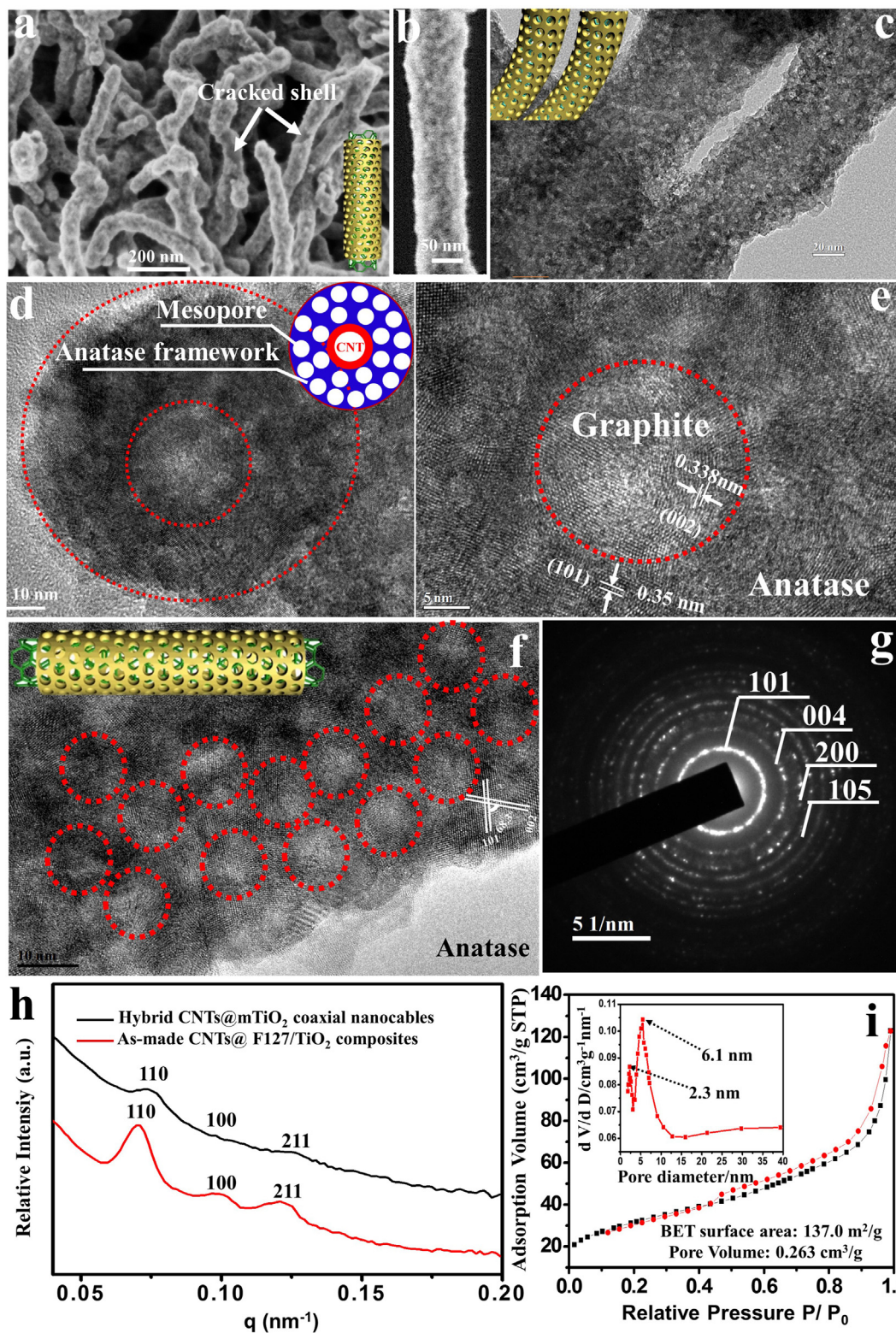
Fig. 2. (a, b) SEM image of the flexible CNTs@mTiO$_2$ hybrid mesoporous nanocables. Inset of (a) is the mesoscopic structure model of the surface of a single CNTs@mTiO$_2$ hybrid mesoporous nanocable. (c), TEM image of flexible CNTs@mTiO$_2$ hybrid mesoporous nanocables. Inset of (c) is the pore arrangement model. (d, e, f), HRTEM images recorded on a single flexible CNTs@mTiO$_2$ hybrid mesoporous nanocable. Insets of (d) and (f) are the mesoscopic structure models. The dotted red circles in (f) represent open pores exposed on the surface of CNTs@mTiO$_2$ hybrid nanocable. (g), SAED pattern recorded on a single flexible CNTs@mTiO$_2$ hybrid mesoporous nanocable. (h) SAXS patterns of the as-made CNT@amorphous F127/TiO$_2$ hybrid nanocables before calcination and the flexible CNTs@mTiO$_2$ hybrid mesoporous nanocables after calcination at 400 °C in Ar for 2 h. (i), Nitrogen adsorption-desorption isotherms and pore size distributions (inset) of the flexible CNTs@mTiO$_2$ hybrid mesoporous nanocables.

assemble with amphiphilic Pluronic F127 into uniform spherical PEO-PPO-PEO/titania oligomer micelles at the mixture solvent of ethanol and DMF [40,54,55]. After the surface functionalization, the CNTs surface is chemically active and can be well dispersed in the ethanol/DMF mixed solution. At a low concentration, the tendency of the spherical F127/TiO$_2$ composite micelles heterogeneous
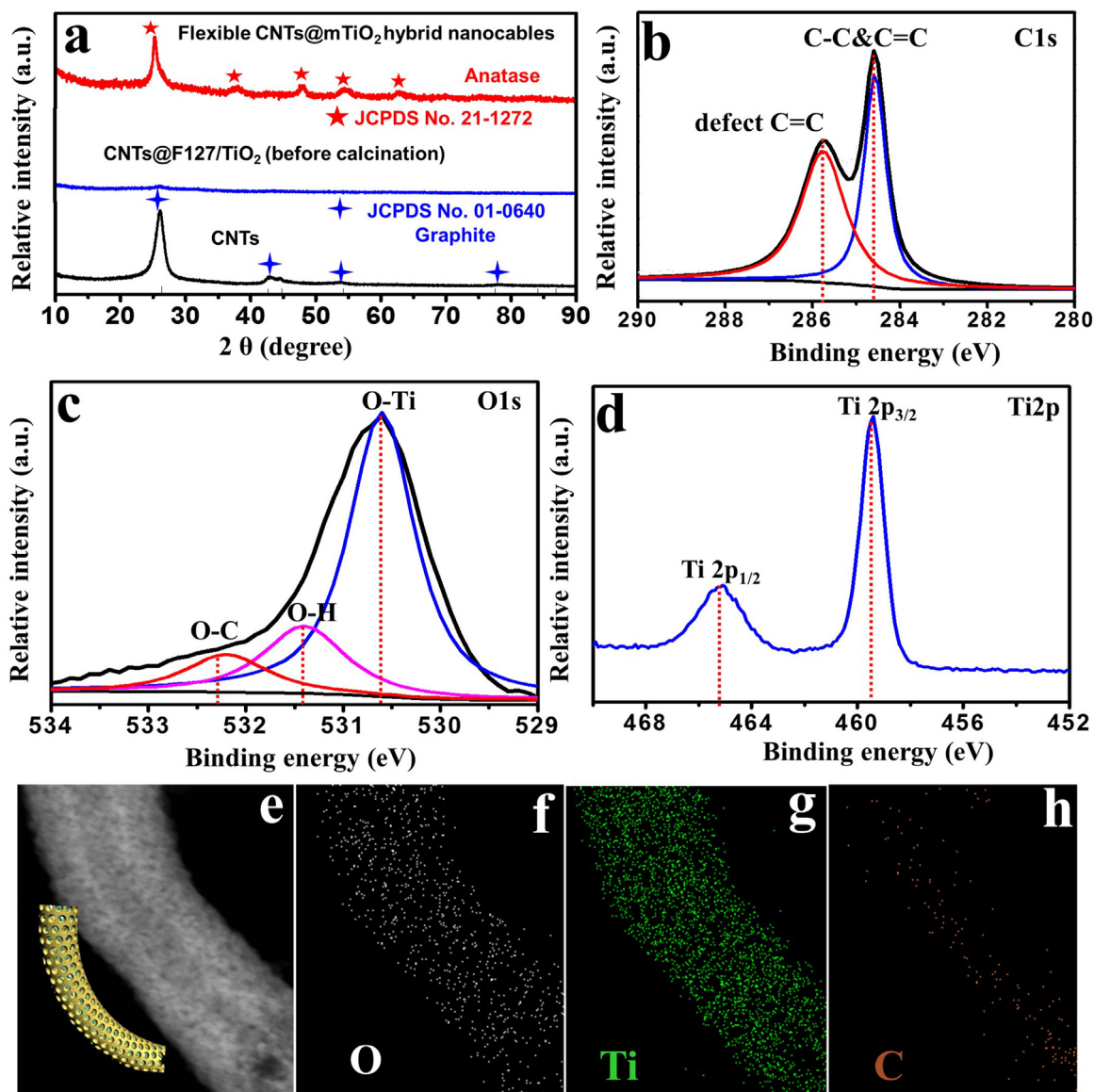
Fig. 3. (a), WXRD patterns of the multi-wall CNTs, the as-made CNT@amorphous F127/TiO$_2$ hybrid nanocables before calcination and the flexible CNTs@mTiO$_2$ hybrid mesoporous nanocables prepared after calcination at 400 °C in Ar for 2 h. (b), C1s, (c), O$_{1s}$ and (d) Ti$_{2p}$ XPS core-level spectra for the flexible CNTs@mTiO$_2$ hybrid mesoporous nanocables (e), STEM image of a single flexible CNTs@mTiO$_2$ hybrid mesoporous nanocable. (f–h), EDX elemental mapping images of a single flexible CNTs@mTiO$_2$ hybrid mesoporous nanocable. White, green, and orange indicate oxygen, titanium and carbon atoms, respectively. (For interpretation of the references to color in this figure legend, the reader is referred to the web version of this article.)

nucleation on the surface of the functionalized CNTs is more favourable than the spontaneous stacking of micelles by homogeneous nucleation. Therefore, in the beginning sol-gel process, the initially formed spherical micelles as subunits can slowly be diffused and selectively anchored at the oxygen functional group sites of the oxidized CNTs owing to their strong hydrogen-bonding interaction. Once the spherical micelles deposition occurs, the new hydrolysed spherical micelles continuously diffuse and layer-by-layer deposit on the functionalized CNTs surface owing to deduction of high interfacial energy, thus resulting in a thin and continuous composite micelle layer on the surface of CNTs. Upon increasing ammonia content (0.3 vol% ammonia), the hydrolysis and condensation of TBOT can be promoted. In this case, the plentiful of spherical F127/TiO$_2$ composite micelles are formed, making the TiO$_2$ shells rapidly grow in thickness through a layer-by-layer coating. However, with a much higher content (> 0.4 vol%) or lower content (< 0.2 vol%) of ammonia, the balance between the production and consumption of spherical composite micelles is broken, thus

resulting in isolated TiO$_2$ nanospheres or non-uniform TiO$_2$ coating. Without F127 templating assembly, only heterogeneous nucleation of TiO$_2$ nanoparticles takes place on the surface of CNTs, resulting in continuous TiO$_2$ nanoparticles coating layer on the surface of CNTs (CNTs@TiO$_2$ NPs).

We further demonstrate that ultrathin mesoporous TiO$_2$ shells can also be uniformly coated on the planar surfaces of the graphene (GR) via this surfactant-templating assembly coating method (Fig. 4a). The graphene nanoflakes can be uniformly coated by two ultrathin mesoporous TiO$_2$ layers (top and bottom) with an average thickness of ~11 nm, resulting in a uniform sandwich-like flexible GR@mTiO$_2$ nanoflakes (Fig. 4b and c). The average spherical pore size is estimated to be ~8 nm. The HRTEM and SAED pattern confirm that the mesoporous TiO$_2$ shells are well crystallized in anatase phase (Fig. 4d). The Raman spectrum indicates the characteristic peaks of anatase TiO$_2$ at 154 cm^{-1} and the D band (1342 cm^{-1}) and G band (1586 cm^{-1}) of graphene (Fig. 4e). The atomic force microscopy (AFM) and thickness
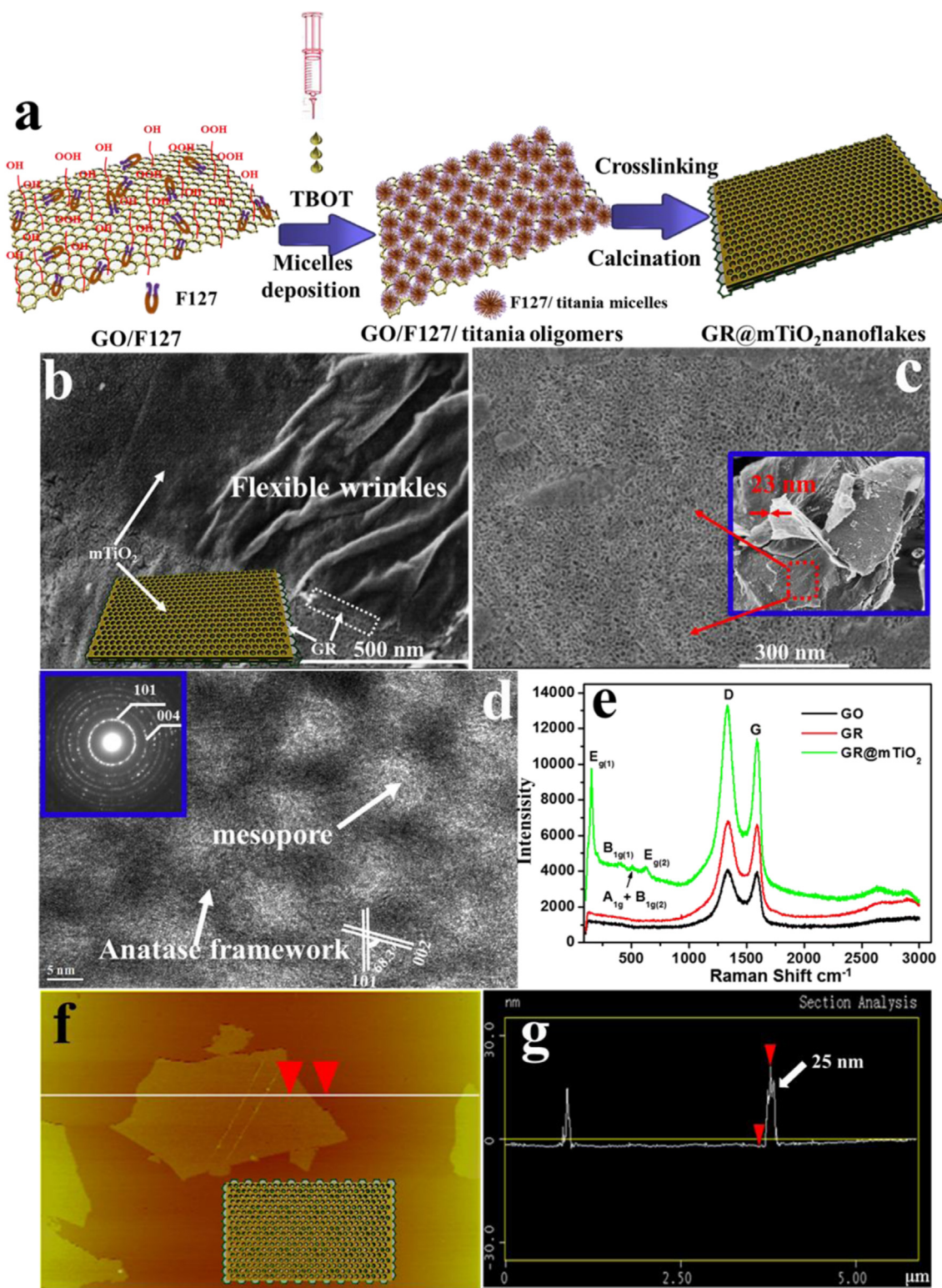
Fig. 4. (a) Schematic representation of the surfactant-templating coating approach for the preparation of the sandwich-like mesoporous GR@mTiO$_2$ hybrid nanoflakes. (b, c) SEM images of GR@mTiO$_2$ hybrid nanoflakes. Inset of (b) is the mesoscopic structure model of the surface of a single GR@mTiO$_2$ hybrid nanoflakes. (d), HRTEM images recorded on the surface of a single GR@mTiO$_2$ hybrid nanoflakes. Insets of (d) is the corresponding SAED pattern. (e), Raman spectra of the graphene oxide (GO), reduced graphene (GR) and GR@mTiO$_2$ hybrid nanoflakes. (f), AFM topography images of the GR@mTiO$_2$ nanoflakes on a mica substrate and (g) the corresponding height-profile analysis along the line in (f).

analyses reveal that the total thickness of the sandwich-like GR@mTiO$_2$ nanoflakes is about 23 nm (Fig. 3f and g), indicating that each mesoporous TiO$_2$ layer exhibits a thickness of about 11 nm, which is consistent with the SEM results.

As a proof of concept, the electrochemical performances of the flexible CNTs@mTiO$_2$ hybrid mesoporous nanocables are investigated

as anode materials for LIBs. The charge-discharge voltage profiles of the flexible CNTs@mTiO$_2$ hybrid mesoporous nanocables electrode at a rate of 20 C (1 C=170 mA g^{-1}) show the first discharge capacity are 260 mA h g^{-1} (Fig. 5(a)). The discharge capacity drops to 158 mA h g^{-1} in the first 10 cycles, which is attributed to the irreversible interfacial reaction between anatase TiO$_2$ and the electrolyte [43].
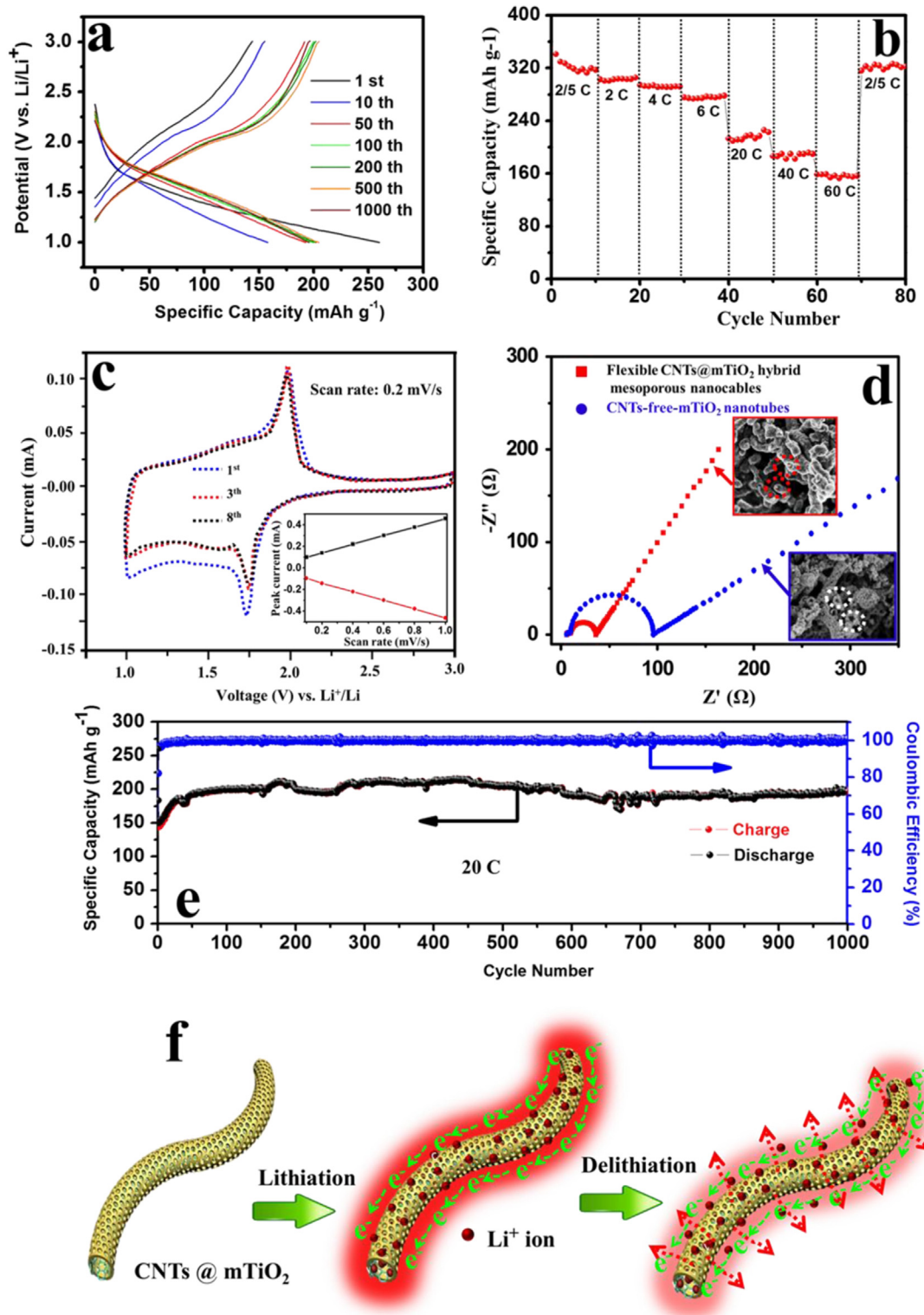
Fig. 5. Electrochemical performance characterization of the flexible CNTs@mTiO$_2$ hybrid mesoporous nanocables. (a), Charge-discharge voltage profiles at a current rate of 20 C. (b), Rate capacity at different current rates from 0.2 C to 60 C. (c), Cyclic voltammogram curves of the CNTs@mTiO$_2$ hybrid mesoporous electrode at a scan rate of 0.2 mV/s. Inset is the plot of peak reduction current with respect to scan rates from 0.1 to 1.0 mV/s. (d), Nyquist plots of the flexible CNTs@mTiO$_2$ hybrid mesoporous nanocables and CNTs-free-mTiO$_2$ nanotubes at room temperature. (e), cycle performance at a constant current rate of 20 C. (f), Schematic representation of the lithiation and delithiation processes of the flexible CNTs@mTiO$_2$ hybrid mesoporous nanocables.

After 50 cycles, the discharge capacity gradually increases to 200 mA h g^{-1} with a corresponding charge capacity of 199 mA h g^{-1}, suggesting a possible activating process in the flexible CNTs@mTiO$_2$ hybrid mesoporous nanocables. The discharge and charge capacities show almost no change during the subsequent 1000 cycles, confirming

excellent stability and high reversibility for the CNTs@mTiO$_2$ hybrid mesoporous nanocables at a high rate (20 C). The discharge and charge profiles deliver a high discharge and charge capacity of about 213 mA h g^{-1} after 1000 cycles, resulting in a high Coulumbic efficiency of nearly 100%. It is worth mentioning that the weight

percentage of TiO_2 in the CNT@mTiO$_2$ hybrid nanocables is dependent on the thickness of the mesoporous TiO_2 layers, which can be tuned in the range of 50–80%. For the best performance on lithium battery, we have optimized the ratio of TiO_2 to be 70% (~20 nm in TiO_2 shell thickness).

To investigate the rate capability, the flexible CNTs@mTiO$_2$ hybrid mesoporous nanocables electrode was discharged and charged at various current rates. The discharge capacity was found to be about 320, 300, 290, 270, 210, 180 and 150 mA h g^{-1} at current rates of 0.4, 2, 4, 6, 20, 40 and 60 C (Fig. 5b), respectively, confirming the excellent electronic/ionic transport properties and improved reaction kinetics. When the current rate was abruptly switched back to 0.4 C, a stable high capacity of about 320 mA h g^{-1} was recovered, confirming the excellent stability and reversibility of the CNTs@mTiO$_2$ hybrid mesoporous nanocables. Even at ultra-high rate of 60 C (Fig. 5b), the capacity of this lithium-ion cell can reach around 160 mA h g^{-1}. The cyclic voltammogram (CV) curve of the CNTs@mTiO$_2$ hybrid electrode shows two peaks at 1.73 V (cathodic) and 1.97 V (anode), which are associated with Li$^+$ insertion/extraction in the anatase lattice (Fig. 5c) [26]. The CV curves show an ideal rectangular shape in the range of 1.0–1.7 V, which is the characteristic of pseudocapacitive storage behaviour contributed from the ultrathin mesoporous TiO_2 shells. The CV measurements at different scan rates of 0.1–1.0 mV/s (the inset of Fig. 5c) also clearly show that the peak current varies linearly with the scan rate, which further confirms the fast pseudocapacitive charge storage process in the CNTs@mTiO$_2$ hybrid electrode. For charge transfer resistance (R$_{ct}$) comparison, a CNTs-free-mTiO$_2$ sample is prepared by removing CNT cores of CNTs@mTiO$_2$ hybrid mesoporous nanocables via calcination in air at 400 °C for 3 h. Nyquist plots of the flexible CNTs@mTiO$_2$ hybrid mesoporous nanocables and CNTs-free-mTiO$_2$ nanocubes after removal of the CNTs by calcination at 500 °C in air show a semicircle in the moderate frequency region and a straight line in the high frequency region (Fig. 5d), which are relevant to a charge transfer process and Warburg diffusion process [27], respectively. Compared to CNTs-free-mTiO$_2$ nanocubes (R$_{ct}$, 86 Ω), the flexible CNTs@mTiO$_2$ hybrid mesoporous nanocables show much lower charge transfer resistance (R$_{ct}$, 27 Ω) in the moderate frequency region, confirming that the lithium ions and electrons' transfer can be dramatically increased in the CNTs@mTiO$_2$ hybrid nanocables.

The flexible CNTs@mTiO$_2$ hybrid mesoporous nanocable electrode exhibits superior cycling capacity (about 210 mA h g^{-1}) over 1000 cycles at a high rate of 20 C accompanied with nearly 100% Coulombic efficiency (Fig. 5e). The SEM image of flexible CNTs@mTiO$_2$ hybrid mesoporous nanocables after cycling at 20 C for 500 cycles shows no notable variation in morphology or collapse of the hybrid structure (Fig. S9), confirming its excellent tolerance of ultrafast lithium ions insertion and extraction for long-life LIBs. Compared to the flexible CNTs@mTiO$_2$ hybrid mesoporous nanocables, it is worth noting that the CNTs@TiO$_2$ NPs hybrid nanocables obtained without Pluronic F127 template show much lower rate capability of only about 80 mA h g^{-1} at a current rate of 20 C (Fig. S10). The lower rate capability of the CNTs@TiO$_2$ NPs hybrid nanocables is possibly attributed to their lower BET surface area (87 m^2/g) and pore volume (0.17 cm^3/g). For further comparison, Fig. S10 shows the rate-capability performance of the CNTs@mTiO$_2$ hybrid mesoporous nanocables (our work) and some other CNT/TiO$_2$ composites reported previously. It should be noted that the rate capability from our nanocables is much higher than that for other hybrid nanostructures, such as CNT/TiO$_2$ nanocrystals [56], CNT/TiO$_2$ nanosheets [33], CNT/TiO$_2$ nanoparticles [32] and CNT@ nanoporous TiO$_2$ coaxial nanocables [29] under similar testing conditions. In addition, the discharge capacity of the obtained mesoporous GR@mTiO$_2$ nanoflakes was measured to be about 310, 290, 275, 265, 205, 165 and 145 mA h g^{-1} at current rates of 0.4, 2, 4, 6, 20, 40 and 60 C (Fig. S10), respectively. It is a little lower than that of the CNTs@mTiO$_2$ hybrid mesoporous nanocables, but still higher than the values from other CNT/TiO$_2$ hybrid nanocomposites (such as CNT/TiO$_2$

nanocrystals [56], CNT/TiO$_2$ nanosheets [33], CNT/TiO$_2$ nanoparticles [32] and CNT@ nanoporous TiO$_2$ coaxial nanocables [29]) reported previously.

The remarkable high-rate capability and superior cycling stability of the flexible CNTs@mTiO$_2$ hybrid mesoporous nanocable can mainly be attributed the synergistic coupling effects between graphitic CNTs, high surface area, accessible large pores and highly crystalline thin mesoporous shells. The thin mesoporous crystalline TiO_2 shells with a large surface area and accessible large mesopore (~6.2 nm) can not only provide large active surface sites, but also greatly reduces Li$^+$ diffusion length and guarantees the fast kinetics for Li$^+$ insertion and de-insertion, leading to a high-rate capacity. On the other hand, the graphitic CNTs core can significantly improve the electronic conductivity between the mesoporous anatase TiO_2 shells and current collectors, thus giving rise to high-rate capacity. The robust core-shell mesostructure effectively prevents the undesirable aggregation and volume expansion upon the lithiation and delithiation, which give rise to a long cycle life performance. Additionally, the highly crystalline nature of the mesoporous anatase TiO_2 shells can also contribute to the electrical conductivity and crystal lattice robustness during repeated charge-discharge cycling. The above outstanding features probably promote the electrochemical process and lead to high specific rate capability and superior cyclability.

4. Conclusions

In summary, well-defined, uniform flexible CNTs@mTiO$_2$ hybrid mesoporous nanocables with thin crystalline anatase shell and accessible mesopores have successfully been synthesized by a novel surfactant-templating assembly coating approach. This surfactant-templating assembly coating approach experiences a controlled layer-by-layer spherical F127/TiO$_2$ composite micelles coating process, and the thickness of the mesoporous TiO_2 shell can be well tuned from ~20 to ~60 nm by adjusting the spherical composite micelles content and ammonia concentration. Typically, the flexible CNTs@mTiO$_2$ hybrid mesoporous nanocable with ~20 nm shell thickness show an ultra-high surface area (~137 m^2/g), large internal pore volume (~0.26 cm^3/g), uniform accessible mesopores (~6.2 nm) and highly crystalline mesoporous anatase shells frameworks. Owing to their above unique features as well as synergistic coupling effect, the CNTs@mTiO$_2$ shows ultrahigh-rate capacity (~210 mA h g^{-1} at 20 C), perfect coulombic efficiency (nearly 100%) and superior cycling stability (keeping high capacity of ~210 mA h g^{-1} after 1000 cycles at 20 C). This surfactant-templating assembly coating approach can be easily extended to deposit an ultrathin mesoporous TiO_2 layer on flat graphene, which opens up a new design for depositing thin mesoporous transition-metal oxides on graphitized carbon supports for advanced applications in energy conversion and storage, photocatalysis, sensors and drug delivery, etc.

Appendix A. Supplementary material

Supplementary data associated with this article can be found in the online version at http://dx.doi.org/10.1016/j.nanoen.2016.04.028.

References

[1] Y. Tang, Y. Zhang, J. Deng, J. Wei, H.L. Tam, B.K. Chandran, Z. Dong, Z. Chen, X. Chen, Adv. Mater. 26 (2014) 6111–6118.
[2] C.K. Chan, H. Peng, G. Liu, K. McIlwrath, X.F. Zhang, R.A. Huggins, Y. Cui, Nat. Nanotechnol. 3 (2008) 31–35.
[3] J. Jiang, Y. Li, J. Liu, X. Huang, C. Yuan, X.W.D. Lou, Adv. Mater. 24 (2012) 5166–5180.
[4] B. Kang, G. Ceder, Nature 458 (2009) 190–193.
[5] D. Dubal, O. Ayyad, V. Ruiz, P. Gómez-Romero, Chem. Soc. Rev. 44 (2015) 1777–1790.
[6] N. Li, Z. Chen, W. Ren, F. Li, H.-M. Cheng, Proc. Natl. Acad. Sci. 109 (2012) 17360–17365.
[7] P. Simon, Y. Gogotsi, Nat. Mater. 7 (2008) 845–854.
[8] J.W. Long, M.B. Sassin, A.E. Fischer, D.R. Rolison, A.N. Mansour, V.S. Johnson, P. E. Stallworth, S.G. Greenbaum, J. Phys. Chem. C 113 (2009) 17595–17598.
[9] Z.S. Wu, W. Ren, D.W. Wang, F. Li, B. Liu, H.M. Cheng, ACS Nano 4 (2010) 5835–5842.
[10] C.X. Guo, M. Wang, T. Chen, X.W. Lou, C.M. Li, Adv. Energy Mater. 1 (2011) 736–741.
[11] J.S. Chen, Y.L. Cheah, Y.T. Chen, N. Jayaprakash, S. Madhavi, Y.H. Yang, X.W. Lou, J. Phys. Chem. C 113 (2009) 20504–20508.
[12] H. Liu, D. Su, G. Wang, S.Z. Qiao, J. Mater. Chem. 22 (2012) 17437–17440.
[13] H. Liu, S. Chen, G. Wang, S.Z. Qiao, Chem. Eur. J. 19 (2013) 16897–16901.
[14] L. Xia, S. Wang, G. Liu, L. Ding, D. Li, H. Wang, S. Qiao, Small 12 (2016) 853–859.
[15] S. Chen, G. Liu, H. Yadegari, H. Wang, S.Z. Qiao, J. Mater. Chem. A 3 (2015) 2559–2563.
[16] H. Liu, D. Su, R. Zhou, B. Sun, G. Wang, S.Z. Qiao, Adv. Energy Mater. 2 (2012) 970–975.
[17] Y. Tang, Y. Zhang, W. Li, B. Ma, X. Chen, Chem. Soc. Rev. 44 (2015) 5926–5940.
[18] Q. Zhang, E. Uchaker, S.L. Candelaria, G. Cao, Chem. Soc. Rev. 42 (2013) 3127–3171.
[19] Van der Ven, J. Bhattacharya, A.A. Belak, Acc. Chem. Res. 46 (2012) 1216–1225.
[20] H. Zhang, X. Yu, P.V. Braun, Nat. Nanotechnol. 6 (2011) 277–281.
[21] L. Zhou, D. Zhao, X.W. Lou, Adv. Mater. 24 (2012) 745–748.
[22] D. Wang, D. Choi, J. Li, Z. Yang, Z. Nie, R. Kou, D. Hu, C. Wang, L.V. Saraf, J. Zhang, ACS Nano 3 (2009) 907–914.
[23] J.S. Chen, H. Liu, S.Z. Qiao, X.W.D. Lou, J. Mater. Chem. 21 (2011) 5687–5692.
[24] J. Zhu, T. Zhu, X. Zhou, Y. Zhang, X.W. Lou, X. Chen, H. Zhang, H.H. Hng, Q. Yan, Nanoscale 3 (2011) 1084–1089.
[25] J.S. Chen, Y. Zhang, X.W. Lou, ACS Appl. Mater. Interfaces 3 (2011) 3276–3279.
[26] S. Ding, J.S. Chen, Adv. Funct. Mater. 21 (2011) 4120–4125.
[27] H. Liu, W. Li, D. Shen, D. Zhao, G. Wang, J. Am. Chem. Soc. 137 (2015) 13161–13166.
[28] B. Wang, H. Xin, X. Li, J. Cheng, G. Yang, F. Nie, Sci. Rep. 4 (2014) 3729.
[29] L. He, C. Wang, X. Yao, R. Ma, H. Wang, P. Chen, K. Zhang, Carbon 75 (2014) 345–352.
[30] J. Wang, R. Ran, M.O. Tade, Z. Shao, J. Power Sources 254 (2014) 18–28.
[31] F.F. Cao, Y.G. Guo, S.F. Zheng, X.L. Wu, L.Y. Jiang, R.R. Bi, L.J. Wan, J. Maier, Chem. Mater. 22 (2010) 1908–1914.
[32] J. Wang, R. Ran, M.O. Tade, Z. Shao, J. Power Sources 254 (2014) 18–28.
[33] S. Ding, J.S. Chen, X.W. Lou, Adv. Funct. Mater. 21 (2011) 4120–4125.
[34] W. Li, F. Wang, S. Feng, J. Wang, Z. Sun, B. Li, Y. Li, J. Yang, A.A. Elzatahry, Y. Xia, D.,Y. Zhao, J. Am. Chem. Soc. 135 (2013) 18300–18303.
[35] W. Li, F. Wang, Y. Liu, J. Wang, J. Yang, L. Zhang, A.A. Elzatahry, D. Al-Dahyan, Y. Xia, D.Y. Zhao, Nano Lett. 15 (2015) 2186–2193.
[36] X. Huang, X. Qi, F. Boey, H. Zhang, Graphene-Based Compos. Chem. Soc. Rev. 41 (2012) 666–686.
[37] Q. Xiang, J. Yu, M. Jaroniec, Chem. Soc. Rev. 41 (2012) 782–796.
[38] X. Li, W. Qi, D. Mei, M.L. Sushko, I. Aksay, J. Liu, Adv. Mater. 24 (2012) 5136–5141.
[39] D. Wang, R. Kou, D. Choi, Z. Yang, Z. Nie, J. Li, L.V. Saraf, D. Hu, J. Zhang, G. L. Graff, ACS Nano 4 (2010) 1587–1595.
[40] Y. Liu, R. Che, G. Chen, J. Fan, Z. Sun, Z. Wu, M. Wang, B. Li, J. Wei, Y. Wei, G. Wang, G.Z. Guan, A.A. Elzatahry, A.A. Bagabas, A.M. Al-Enizi, Y.H. Deng, H. S. Peng, D.Y. Zhao, Sci. Adv. 1 (2015) e1500166.
[41] Y. Liu, Y. Luo, A.A. Elzatahry, W. Luo, R. Che, J. Fan, K. Lan, A.M. Al-Enizi, Z. Sun, B. Li, Z.W. Liu, D.K. Shen, Y. Ling, C. Wang, J.X. Wang, W.J. Gao, C. Yao, K.P. Yuan, H.S. Peng, Y. Tang, Y.H. Deng, G.F. Zheng, G. Zhou, D.Y. Zhao, ACS Cent. Sci. 1 (2015) 400–408.
[42] Y. Liu, K. Lan, A.A. Bagabas, P. Zhang, W. Gao, J. Wang, Z. Sun, J. Fan, A. A. Elzatahry, D. Zhao, Small 12 (2016) 860–867.
[43] J.S. Chen, Y.L. Tan, C.M. Li, Y.L. Cheah, D. Luan, S. Madhavi, F.Y.C. Boey, L. A. Archer, X.W. Lou, J. Am. Chem. Soc. 132 (2010) 6124–6130.
[44] E.J. Crossland, N. Noel, V. Sivaram, T. Leijtens, J.A. Alexander-Webber, H. J. Snaith, Nature 495 (2013) 215–219.
[45] H.G. Yang, C.H. Sun, S.Z. Qiao, J. Zou, G. Liu, S.C. Smith, H.M. Cheng, G.Q. Lu, Nature 453 (2008) 638–641.
[46] H.G. Yang, G. Liu, S.Z. Qiao, C.H. Sun, Y.G. Jin, S.C. Smith, J. Zou, H.M. Cheng, G. Q. Lu, J. Am. Chem. Soc. 131 (2009) 4078–4083.
[47] Y. Liu, L. Chen, J. Hu, J. Li, R. Richards, J. Phys. Chem. C 114 (2010) 1641–1645.
[48] B. Liu, H.C. Zeng, Chem. Mater. 20 (2008) 2711–2718.
[49] Y. Cong, X. Li, Y. Qin, Z. Dong, G. Yuan, Z. Cui, X. Lai, Appl. Catal. B-Environ. 107 (2011) 128–134.
[50] J. Li, S. Tang, L. Lu, H.C. Zeng, J. Am. Chem. Soc. 129 (2007) 9401–9409.
[51] L.-C. Chen, Y.-C. Ho, W.-S. Guo, C.-M. Huang, T.-C. Pan, Electrochim. Acta 54 (2009) 3884–3891.
[52] D.Y. Deng, Y. Cai, Z. Sun, J. Liu, C. Liu, J. Wei, W. Li, C. Liu, Y. Wang, D.Y. Zhao, J. Am. Chem. Soc. 132 (2010) 8466–8473.
[53] Y. Deng, D. Qi, C. Deng, X. Zhang, D. Zhao, J. Am. Chem. Soc. 130 (2008) 28–29.
[54] M. Wang, X. Wang, Q. Yue, Y. Zhang, C. Wang, J. Chen, H. Cai, H. Lu, A. A. Elzatahry, D. Zhao, Chem. Mater. 26 (2014) 3316–3321.
[55] M. Wang, Z. Sun, Q. Yue, J. Yang, X. Wang, Y. Deng, C. Yu, D. Zhao, J. Am. Chem. Soc. 136 (2014) 1884–1892.
[56] Z. Chen, D. Zhang, X. Wang, X. Jia, F. Wei, H. Li, Y. Lu, Adv. Mater. 24 (2012) 2030–2036.

Dr. Yong Liu received his Ph. D. degree from Fudan University in 2015. Now, he is a postdoctoral fellow with Prof. Dongyuan Zhao in Laboratory of Advanced Materials, Fudan University. His research interests focus on the synthesis of oriented mesoporous semiconductors for energy storage and conversion.

Dr. Ahmed A. Elzatahry now is an associate professor in materials science and technology program, college of arts and sciences, Qatar University, He received the award for The State Prize of Egypt in Advanced science and technology (Chemistry) in 2010. In 2006, he moved to the United States-Virginia Commonwealth University (VCU) as a research scholar to take advantage of work in nanotechnology and its application in catalysis field. In 2007, He received his Ph. D. from al-Azhar University, Egypt. In 2008 and 2009 he undertook postdoctoral work in porous and mesoporous materials at VCU, USA.

Dr. Wei Luo is now a lecturer in the State Key Laboratory for Modification of Chemical Fibers and Polymer Materials, College of Materials Science and Engineering at Donghua University. He obtained the Bachelor (2006) and Master (2009) degree at Nanjing Tech University (China). He received his Ph. D. in chemistry in 2014 from Fudan University supervised by Professor Dongyuan Zhao. He received the second prize of Natural Science Award of Ministry of Education (the first awardee). His research interests mainly include the synthesis of functional mesoporous and nanomaterials for energy storage and conversion as well as sensors.

Mr. Pengfei Zhang received his Bachelor degree from Wuhan University of Technology in 2015. Now, he is a Ph.D. candidate in Laboratory of Advanced Materials, Fudan University. His research interests focus on the synthesis of mesoporous semiconductors for energy storage.
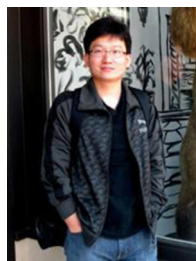
Mr. Kun Lan received his Bachelor degree from Lanzhou University in 2013. Now, he is a Ph.D. candidate in Laboratory of Advanced Materials, Fudan University. His research interests include synthesis of mesoporous semiconductors for energy storage and conversion.

Dr. Jianwei Fan is an associate professor in College of Environmental Science and Engineering at Tongji University. He completed his Post-doctoral research in Laboratory of Advanced Materials in 2014, Fudan University. His current research interests focus on the novel materials for energy and environmental science.

Prof. Fan Zhang received his Ph. D. in 2008 from Fudan University followed by more than 2 years postdoctoral experience in University of California at Santa Barbara before joining as an associate professor in the Chemistry Department of Fudan University in 2010. He became a full professor in Fudan University in 2013. His current research interests include the development of multifunctional nanostructured materials and nanotechnology for applications in biomedical analysis, drug delivery and cancer therapy.

Mr. Wei Yong received his Master degree from Fudan University in 2010. Now, he is a Ph. D. candidate in Laboratory of Advanced Materials, Fudan University. His research interests mainly focus on the synthesis and application for ordered mesoporous materials.
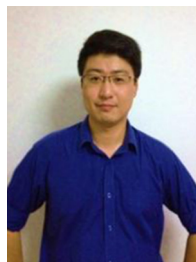
Prof. Yun Tang received his B. S. degree in Chemical Physics in 2003 from University of Science and Technology of China (USTC), and his Ph. D. degree from University of Maryland, College Park in 2009. He joined Department of Chemistry at Fudan University in 2014 as a professor. Prof. Tang's research has focused primarily on precise and tunable controlling of nanostructures, aimed at serving as model systems to explore fundamental science.

Mr. Chun Wang received his Master degree from Fudan University in 2014. Now, he is a Ph. D. candidate in Department of Chemistry, Fudan University. His research interests mainly focus on the synthesis and application for ordered mesoporous materials.
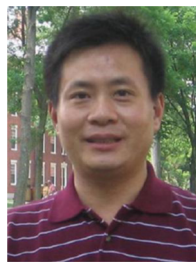
Prof. Liqiang Mai is Chair Professor of Materials Science and Engineering at Wuhan University of Technology and Executive Director of WUT-Harvard Joint Nano Key Laboratory. He received his Ph. D. from Wuhan University of Technology in 2004. He carried out his postdoctoral research in the laboratory of Prof. Zhonglin Wang at Georgia Institute of Technology in 2006–2007 and worked as advanced research scholar in the laboratory of Prof. Charles M. Lieber at Harvard University in 2008–2011. His current research interests focus on nanowire materials and devices for energy storage.

Prof. Yonghui Deng received his B. S. in chemistry from Nanchang University (2000) and Ph. D. in polymer chemistry & physics from Fudan University (2005). He worked as a postdoctoral researcher with Prof. Dongyuan Zhao (2005–2007), and was promoted as associate (2007) and full professor (2011) in Fudan University. He has coauthored over 60 scientific papers and filed 12 patents. His research interests include core–shell nanomaterials, functional porous materials, and their applications in catalysis, and separation, etc.

Prof. Dongyuan Zhao is a Chair Professor of Materials and Chemistry (Cheung Kong and Hao Qing Professorship), and a Director of the Laboratory of Advanced Materials at Fudan University (China). He is also the Co-Director of the 2011 Collaborative Innovation Center of Chemistry for Energy Materials (iChEM). He received his B. S. (1984) and Ph. D. (1990) from Jilin University. He carried out postdoctoral research at the Weizmann Institute of Science (1993–1994), University of Houston (1995–1996), and University of California at Santa Barbara (1996–1998). He was elected as an academician the Chinese Academy of Science in 2007, and a member of The World Academy of Science (TWAS) in 2010. His research interests are focused on the interfacial assembly and macroscopic control of ordered mesoporous materials for applications in catalysis, energy, water purification and biomedicine.

Prof. Gengfeng Zheng obtained his B. S. degree (2000) at Fudan University in China, and Master (2004) and Ph. D. (2007) degrees in Chemistry at Harvard University in USA, under the guidance of Prof. Charles Lieber. He was a postdoctoral fellow working with Prof. Chad Mirkin at Northwestern University in USA (2007–2009). He became a full professor at the Department of Chemistry and Laboratory of Advanced Materials at Fudan University in 2010. He is also a Co-Editor of the Journal of Colloid and Interface Science, and an Advisory Board member of the Journal of Materials Chemistry A. His research interests include low-dimensional semiconducting nanomaterial-based synthesis and surface chemistry, biosensing, interfacing with cells, photoelectrochemical conversion, photocatalysis and energy storage.